GA–A25660

QUANTITATIVE RADIOGRAPHY: SUBMICRON DIMENSION CALIBRATION FOR ICF ABLATOR SHELL CHARACTERIZATION

by

H. HUANG, B.J. KOZIOZIEMSKI,* R.B. STEPHENS, A. NIKROO,
S.A. EDDINGER, K.C. CHEN, H.W. XU, and K.A. MORENO

JANUARY 2007

DISCLAIMER

This report was prepared as an account of work sponsored by an agency of the United States Government. Neither the United States Government nor any agency thereof, nor any of their employees, makes any warranty, express or implied, or assumes any legal liability or responsibility for the accuracy, completeness, or usefulness of any information, apparatus, product, or process disclosed, or represents that its use would not infringe privately owned rights. Reference herein to any specific commercial product, process, or service by trade name, trademark, manufacturer, or otherwise, does not necessarily constitute or imply its endorsement, recommendation, or favoring by the United States Government or any agency thereof. The views and opinions of authors expressed herein do not necessarily state or reflect those of the United States Government or any agency thereof.

GA–A25660

QUANTITATIVE RADIOGRAPHY: SUBMICRON DIMENSION CALIBRATION FOR ICF ABLATOR SHELL CHARACTERIZATION

by
H. HUANG, B.J. KOZIOZIEMSKI,* R.B. STEPHENS, A. NIKROO,
S.A. EDDINGER, K.C. CHEN, H.W. XU, and K.A. MORENO

This is a preprint of a paper presented at the 17th Target Fabrication Specialist Meeting, San Diego, California on October 1-5, 2006 and to be published in *Fusion Science and Technology.*

*Lawrence Livermore National Laboratory, Livermore, California.

Work supported by
the U.S. Department of Energy
under DE-AC52-06NA27279

GENERAL ATOMICS PROJECT 30272
JANUARY 2007

QUANTITATIVE RADIOGRAPHY: SUBMICRON DIMENSION CALIBRATION FOR ICF ABLATOR SHELL CHARACTERIZATION

H. Huang,[1] B.J. Kozioziemski,[2] R.B. Stephens,[1] A. Nikroo,[1] S.A. Eddinger,[1]
K.C. Chen,[1] H.W. Xu,[1] and K.A. Moreno[1]

[1]General Atomics, P.O. Box 85608, San Diego, California 92186-5608
[2]Lawrence Livermore National Laboratory, P.O. Box 808, Livermore, California 94551
huang@fusion.gat.com

National Ignition Facility (NIF) ignition target specifications require submicron dimensional measurement accuracy for the spherical ablator shell, which requires the proper corrections of various distortions induced by the imaging lens, the point projection geometry, and x-ray refraction. The procedures we developed allow measurement accuracies of 0.5 μm for the capsule diameter, ±0.2 μm for the out-of-round (which is the amplitude of the radius variations), ±0.3 μm for the wall thickness (including each sub-layer), and ±0.1 μm for wall thickness profile.

I. INTRODUCTION

Current NIF ignition target designs call for a spherical beryllium shell composed of several doped layers as the ablator (Fig. 1). These ablators have very tight tolerances on the radii, thicknesses, and thickness variations of each of the sublayers, which require dimensional measurements to submicron accuracy. Beryllium is optically opaque which necessitates the use of x-ray imaging to measure the layer thicknesses. Over the last two years, we have developed the imaging equipment and analysis techniques needed to make film-based contact x-radiography quantitative for both dimensional and dopant measurements. Accuracy better than required for NIF ablator dopant level characterization has been demonstrated.[1] This paper updates recent progress in dimensional measurements. We will discuss the error mechanisms in film plate imaging and the correction methods.

II. ERROR MECHANISMS IN DIMENSION MEASUREMENT

Our experimental apparatus consists of an x-ray chamber for radiography and a digitizer to analyze the film image. A conventional x-ray tube with 500 μm spot size is used to expose 2 mm diameter shells resting on a film plate. The source is placed one meter away to reduce the penumbral blurring to approximately 0.5 μm. An emulsion-on-glass film plate is chosen as the x-ray photon detector. This film plate is used because it is very flat which accommodates the limited depth of field of the digitizer, it has sub-micron grain size necessary to achieve high resolution imaging, and it has a large dynamic range necessary to capture intensity information in a single exposure. The film image is digitized after the exposure by using a microscope-mounted Charge-Coupled Device (CCD) camera. The equipment design considerations and the method to remove the pincushion distortion in digitized images were described in an earlier publication.[1] With careful treatment, the typical ~3 μm pincushion distortion can be verifiably reduced to ~0.2 μm.

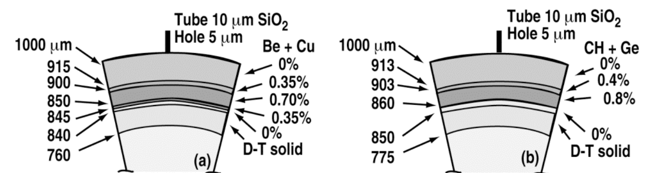

Figure 1. Two alternative NIF target designs utilizing graded ablators: (a) Cu doped Be, (b) Ge doped CH. The "%" values indicate the respective dopant concentrations in atomic percent.

Standard contact radiography analysis methods typically assume that the x-ray photons travel in straight lines through an object, producing an x-ray shadow image that faithfully reproduces the three-dimensional object. That assumption may fail at a submicron level. For example, Fig. 2 shows typical imaging artifacts on a Cr-steel ball known to be round to ±0.1 μm. The expected circular shape is distorted into an ellipse, which is the source of the mode-2 distortion in the Fourier analysis of the radii and the slightly magnified average diameter. There are three effects that cause discrepancy between the image and the shell itself. First, projection from a point source leads to a slight magnification of the sphere diameter,

typically ~2 μm for our imaging geometry. Second, when the shell is not on the imaging axis defined by the point source and the film plate, the x-ray projection effect is position dependent, leading to an elliptical shadow that changes both the shape and the diameter by ~1 μm. Third, the x-rays are subject to refraction and diffraction, sometimes referred to as a phase contrast effect in the literature, that can shift the apparent interface location and affect the wall thickness measurement by ~1 μm. Each of these three effects can be calculated and used to correct the image as described below.

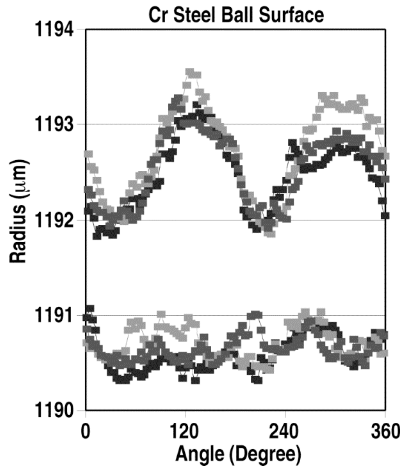

Figure 2. Most shell shadows have a strong mode-2 pattern which is a measurement artifact. In this example, the top 3 traces were measured from a chromium-steel ball with 0.1 μm 1-σ NIST-traceable Out-of-Round (OOR), radiographed 3 times on 3 separate film plates with the same equator orientation. The bottom 3 traces were after corrections for magnification and tilting, showing the true OOR to ±0.25 μm 1-σ standard deviation.

As shown in Fig. 3, the film plate is a distance L from the x-ray source, and the shell center is a distance r from the film plate, where r is the shell radius. The magnification factor for all dimensions is r/L. In our apparatus, with L to be 960 mm, the effect is approximately 0.1% and easy to correct.

The film plate is 100 mm x 125 mm in size. It allows 12 ablator shells, each in it own X-ray Fluorescence (XRF) holder, to be exposed for x-ray simultaneously. A XRF holder is a hollow plastic tube in which a shell is held between two 4 μm thick Mylar films to prevent rolling. The thin Mylar will transmit greater than 50% of the 2 keV and higher x-rays. The film plate center is located on the cylindrical axis of the vacuum chamber where the incoming x-ray is at normal incidence. The multitude of the shells ensures that no more than one shell can be at the film plate center. When a shell is displaced by a distance R from the film plate center, as shown in Fig. 3, the tilted projection would cause the shadow to elongate along the radial direction by a magnification factor $0.5\cdot(R/L)^2$. In the orthogonal direction, the shadow dimension remains unchanged, so the radius, averaged over all azimuthal angles, is magnified by half that amount. In our apparatus, when R is 40 mm and L is 960 mm, the effect elongates the shadow by 1.7 μm, which also increases the measured diameter by half the amount or ~0.8 μm. As with the projection magnification, the dimensional changes due to the tilted projection are proportional to the dimensions being measured. In practice, it means the diameter and the shape measurement must be corrected. The impact on the wall thickness is typically too small to warrant a correction unless a very thick coating is being measured. In contrast, the phase contrast effect disproportionally affects the wall thickness measurement. The origin and the correction method for the phase contrast effect will be discussed in the next section.

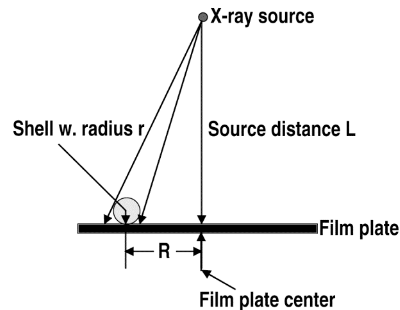

Figure 3. Tilted projection to cause the shadow of the shell to elongate in the radial direction. The typical elongation magnitude is ~1 μm in our experiment.

III. FRESNEL MODELING OF PHASE CONTRAST EFFECT

X-rays are subject to refraction and diffraction, just as visible light, when passing through an object with abrupt changes in the refractive index. In particular, the free-space propagation would enhance the interface contrast of objects when imaged using x-rays.[2-7] These effects have been termed "phase contrast" in x-ray imaging literature. In addition to providing interface contrast enhancement, phase contrast can affect dimensional measurements in two different ways. First, it shifts the apparent positions of the interface, usually due to refraction. Second, it blurs the interface structure to make a precise position determination difficult. These two effects will be discussed.

Phase contrast can be modeled based on Fresnel propagation of the x-ray radiation. One approximation to the Fresnel integral is the so-called thin-object approximation. Starting from a uniform intensity and phase-front, the x-ray phase delay and absorption are calculated

through the object, assuming that the x-rays travel as straight-rays through the object itself. The altered intensity and phase profile are then propagated to the detector. This method has been validated against experimental data.[7] The free-space propagation method can be readily applied to a point source geometry.[8,9] Phase-contrast imaging has proven useful in the study of deuterium-tritium layer characterization[10,11] and was found to be dominated by refractive effects.[10-12] The simulation input parameters are summarized in Table I and an example of the x-ray transmission curve is shown in Fig. 4. The refractive indices of the shell materials are strong functions of x-ray photon energy,[13] which affects the position and the shape of the transmission intensity profile. Therefore, it is necessary to conduct polychromatic simulation with the measured x-ray spectrum.[1]

Table I. Summary of input parameters for Fresnel calculation. System effects due to the x-ray source, the lens and the CCD are deliberately omitted because they will be taken cared of explicitly during system convolution. Projection magnification and tilt elongation, which is easily correctable through a template, is not included.

Simulation Parameters	Value
Be density	1.848 g/cc
CH density	1.05 g/cc
CH composition	C:H = 1:1.35
Be external surface radius	1020.0 μm (or 1100.0 μm)
CH/Be interface radius	1000.0 μm
CH internal surface radius	985.0 μm
Shell center to film plate distance	1.0 mm
X-ray source	9 kV, W-anode, 10 mil Be window

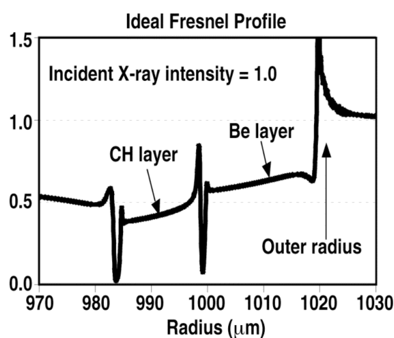

Figure 4. The radial profile of x-ray transmission intensity after the x-ray pass through a beryllium coated CH mandrel under condition outlined in Table I. Sharp spikes in transmission intensity at the interfaces are the hallmark of phase contrast. Please note the intensity just outside the shell is more than the 100% transmission due to phase contrast at the external beryllium surface.

The effect of the source penumbral blurring and the microscope objective lens transfer function (Fig. 5) is included in the simulations by convolving their response with the ideal profile (Fig. 4). The CCD pixel size effect and the film exposure effect are taken into account by performing the radial profiling algorithm developed by Bernat and Stephens[14,15] on simulated 2D image. The analysis technique is identical to the one performed on real images which ensures comparability.

Figure 6(a) shows the radial profile of a simulated image as digitized by a 4× lens. The interface structures have been broadened from the ideal case (Fig. 4). To determine the interface position to submicron accuracy from that structure, it is necessary to pick a marker that can be precisely measured on the profile and to characterize the systematic offset between the marker position and the true interface position. The 2nd derivative of the transmission radial profile is better suitable for interface identification, because it highlights each surface/interface with a peak/valley pair, as shown in Fig. 6(b). In this

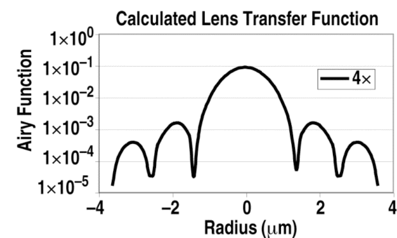

Figure 5. The optical transfer function for a Nikon lens with a numerical aperture of 0.20.

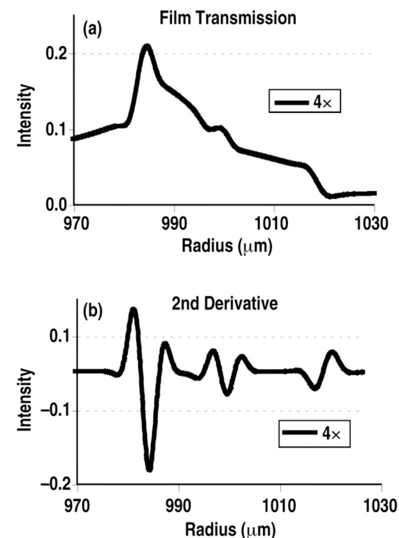

Figure 6. Simulated radial transmission profile and the 2nd derivative profile of a Be/CH shell outlined in Table I. 2nd derivative highlight the surfaces/interfaces and make it easier to identify their locations.

study, we define the mid-point between the peak and the valley on a 2nd derivative curve as the interface marker position. The difference between the interface position (the simulation input) and the marker position (the simulation output) is defined as the phase contrast offset, as shown in Table II.

Table II. An example of how to determine the phase contrast offset. The offset is defined as the difference between the input radius for the simulation and the marker radius. The offset is specific to the digitization instrument and the material composition at the interface. A key finding of the simulation is that the offsets are nearly independent of the layer thicknesses for the typical layers and shells; therefore the input radii used here is of no consequence.

Surface or interface	Input radius (μm)	Marker radius (μm)	Offset (μm)
CH inner surface	985.0	983.0	2.0
Be/CH interface	1000.0	998.5	1.5
Be outer surface	1020.0	1018.9	1.1

We have developed computer software to quickly and reliably pick-up interface marker position to measure the $r(\theta)$ profile of a shell. The wall thickness profile $w(\theta)$ thus determined has a 1-σ repeatability of <±0.1 μm. Repeatability, however, is only a necessary condition for accurate measurement. A systematic study of the marker offset would allow us to obtain the calibration factor to make the measurement accurate.

Following this approach, various Be/CH shell configurations were calculated to answer questions specific to the NIF point target design. The simulation results show that, to an accuracy of approximately ±0.1 μm, the phase contrast offset does not change with the beryllium wall thickness or the oxygen contamination level in the beryllium layer. These observations allow the use of a simple look-up table (Table III) to describe the layer behavior for the entire range of the Be/CH capsule configurations encountered in the NIF program.

IV. VALIDATION

IV.A. Comparison Against CH Shell Standards for Wall Thickness and Wall Thickness Variation

There is no NIST traceable wall thickness standard available, so we used Carbon-Hydrogen Polymer (CH) shells as our calibration standards to check the validity of the phase contrast model. Single-point white-light interference measurements[16] give the wall thickness of CH shells consistent with the radiography measurements. The average discrepancy between the two methods is ~0.3 μm for 25 μm thick CH shells with the within-the-shell wall thickness variation of 0.5 to 1.0 μm (Table IV). Similar comparison can be made against an automated microscope method.[17] A comparison with the spectral-interferometer-based wallmap[18] shows a systematic difference of ~0.6 μm. The layer thickness difference can be understood by the small refractive index uncertainty in the wallmapping data because the wallmapper measures the product of the refractive index and the layer thickness (Table IV). The variations in the wall thickness profile as a function of azimuthal angles, as measured by radiography and by wallmapper, is consistent to the ±0.1 μm repeatability limit of the radiography method (Fig. 7).

Table III. Phase contrast offset (in μm) table for Be/CH shells. This offset table has been incorporated into the Excel template used in production shell characterization. "N/A" indicates where the Be/CH interface is not resolved by the 2X lens.

Interface Type/Lens	2×	4×	10×	20×
Be or CH exterior surface	1.9	1.1	0.4	0.5
Be/CH interface	N/A	1.5	0.7	0.7
Be or CH interior surface	2.7	2.0	1.1	1.1
Be thickness	N/A	-0.4	-0.3	-0.2
CH thickness	N/A	-0.5	-0.4	-0.4
Overall thickness	-0.8	-0.9	-0.7	-0.6

The ability to measure the sublayer interfaces and the interior surface is invaluable to the ICF program. The capability was neatly demonstrated on some novel ICF capsules. Micromachining was used to create a mode-5 pattern on the equator of some PAMS shells. Two set of shells with peak-to-peak sine wave amplitudes of 0.2 μm and 2.0 μm were made. Spheremapper[19] was used characterize the mode-5 pattern and confirm the amplitude had met the specification to 10%. The shells were than coated with a CH layer before the PAMS mandrel was removed in a high-temperature pyrolysis process, during which the mode-5 pattern was transferred to the interior surface of the CH shell. The radiography measurements confirmed the presence of 0.2 μm and 2.0 μm high mode-5 patterns to a ±0.1 μm accuracy before the shells were shipped out for hydrodynamic instability experiment (Fig. 8).

IV.B. Comparison Against Ball Standards for Diameter

The NIST-traceable measurement (±0.3 μm accuracy) performed by the ball manufacturer Ball-Tec Inc. is consistent with the radiography method. Table V shows the chromium steel balls are in agreement with the NIST-

Table IV. Four wall thickness methods compared.
A discussion wallmapper systematic error is found in the text.

Wall Thickness (μm)	Radiography (μm)	Whitelight Interferometry (μm)	Automated Microscope (μm)	Wallmapper Method (μm)
CH2-051305-1	25.1	24.6	24.3	24.5
CH2-051305-2	25.4	25.1	25.4	24.7
CH2-051305-3	25.6	24.9	25.6	24.8
CH2-051305-4	25.4	25.1	24.9	24.6
CH2-051305-5	24.6	24.8	24.3	24.4
Average	25.2	24.9	24.9	24.6

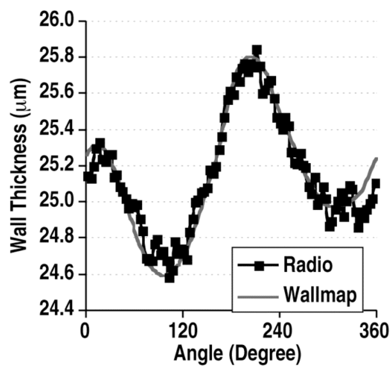

Figure 7. Radiography measurement agrees with wallmapper measurement for CH shell wall thickness profile.

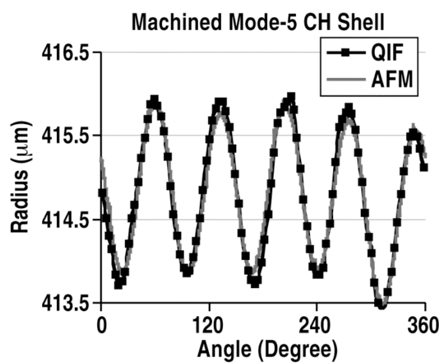

Figure 8. Mode 5 shell highlight radiography method's capability in measuring the interior surface shape.

traceable measurement to ±0.5 μm 1-σ accuracy. Similar measurements on six sapphire balls again prove the accuracy of the radiography method to ±0.5 μm 1-σ accuracy. Combining the phase contrast model with radiography, a very accurate and repeatable method has been developed for measuring the ablator shell dimensions.

V. CONCLUSIONS

Lens distortion, projection magnification, tilted projection and phase contrast are the major error mechanisms in radiographic-based dimensional measurement. With proper calibration, radiography is capable of characterizing ICF capsule dimensions with sub-micron accuracy. Specifically, the diameter can be measured to ±0.5 μm, the shape can be measured to ±0.2 μm, the average wall thickness can be measured to ±0.3 μm, and the variations in the wall thickness as a function of the azimuthal angle can be measured to ±0.1 μm.

Table V. Comparison of the o.d. measurements on six grade-3 chromium steel balls. The balls were NIST-traceably certified to be round to better than ±0.1 μm (which meets the grade-3 definition). Therefore, the ball orientation does not affect diameter measurement by more than ±0.1 μm.

Cr Steel Balls	NIST o.d. (μm)	Radiography (μm)	Difference (μm)
#1	2001.0±0.3	2000.9	-0.1
#2	2001.0±0.3	2000.9	-0.1
#3	2001.0±0.3	2001.0	-0.0
#4	2001.0±0.3	2000.9	-0.1
#5	2001.0±0.3	2000.9	-0.1
#6	2001.0±0.3	2000.4	-0.6
Average	2001.0±0.3	2000.8	-0.2

ACKNOWLEDGMENT

This work was supported by the U.S. Department of Energy under DE-AC52-06NA27279.

REFERENCES

1. H. HUANG, R. B. STEPHENS, S. A. EDDINGER, A. NIKROO, K. C. CHEN, H. W. XU, J. GUNTHER, "Non-destructive Quantitative Dopant Profiling Technique by Contact Radiography," *Fusion Sci. Technol.* **49**, 650 (2006).

2. A. SNIGIREV, I. SNIGIREVA, V. KOHN, S. KUZNETSOV, and I. SCHELOKOV, "On the Possibilities of X-ray Phase Contrast Microimaging

by Coherent High-Energy Synchrotron Radiation," *Rev. Sci. Instrum*. **66**, 5486 (1995).

3. PETER CLOETENS, RAYMOND BARRETT, JOSE BARUCHEL, JEAN-PIERRE GUIGAY, and MICHAEL SCHLENJER, "Phase Objects in Synchrotron Radiation Hard X-ray Imaging," *J. Phys. D* **29**, 133 (1996).

4. S. C. MAYO, P. R. MILLER, S. W. WILKINS, T. J. DAVIS, D. GAO, T. E. GUREYEV, D. PAGANIN, D. J. PARRY, A. POGANY, and A. W. STEVENSON, "Quantitative X-ray Projection Microscopy; Phase-Contrast and Multi-Spectral Imaging," *J. of Microscopy* **207**, 79 (2002).

5. K. A. NUGENT, T. E. GUREYEV, D. F. COOKSON, D. PAGANIN, Z. BARNEA, "Quantitative Phase Imaging Using Hard X Rays," *Phys. Rev. Lett*. **77**, 2961 (1996).

6. S. W. WILKINS, T. E. GUREYEV, D. GAO, A. POGANY, and A. W. STEVENSON, "Phase-Contrast Imaging Using Polychromatic Hard X-rays," *Nature (London)* **384**, 335 (1996).

7. H. E. MARTZ, B. J. KOZIOZIEMSKI, S. K. LEHMAN, S. HAU-RIEGE, D. J. SCHNEBERK, A. BARTY, "Validation of Radiographic Simulation Codes Including X-ray Phase Effects for Millimeter-size Objects With Micrometer Structures," *J. Opt. Soc. Am. A* **24**, 169 (2007).

8. A. POGANY, D. GAO, S. W. WILKINS, "Contrast and Resolution in Imaging With a Microfocus X-ray Source," *Rev. Sci. Instrum*. **68**, 2774 (1997).

9. T. E. GUREYEV, S. W. WILKINS, "On X-ray Phase Imaging With a Point Source," *J. Opt. Soc. Am. A* **15**, 579 (1998).

10. D. S. MONTGOMERY, A. NOBILE, P. J. WALSH, "Characterization of National Ignition Facility Cryogenic Beryllium Capsules Using X-ray Phase Contrast Imaging," *Rev. Sci. Instrum.* **75**, 3986 (2004).

11. B. J. KOZIOZIEMSKI, J. D. SATER, J. D. MOODY, J. J. SANCHEZ, R. A. LONDON, A. BARTY, H. E. MARTZ, D. S. MONTGOMERY, "X-ray Imaging of Cryogenic Deuterium-Tritium Layers in a Beryllium Shell," *J. Applied Physics* **98**, 103105 (2005).

12. B. J. KOZIOZIEMSKI, J. A. KOCH, A. BARTY, H. E. MARTZ, W.-K. LEE, K. FEZZAA, "Quantitative Characterization of Inertial Confinement Fusion Capsules Using Phase Contrast Enhanced X-ray Imaging," *J. Applied Physics* **97**, 063103 (2005).

13. B. L. HENKE, E. M. GULLIKSON, and J. C. DAVIS, "X-ray Interactions: Photoabsorption, Scattering, Transmission, and Reflection at E=50-30000 eV, Z=1-92," *Atomic Data and Nuclear Data Tables* **54**, 181 (1993), as listed at http://www.cxro.lbl.gov/optical_constants/.

14. R. B. STEPHENS, "Precision Shell Characterization Using Radial Averaging of X-ray Images," *J. Vac. Sci. Technol. A* **13**, 979 (1995).

15. D. BERNAT, R. B. STEPHENS, "Algorithm for Better X-radiography Analysis," *Fusion Technol*. **31**, 473 (1997).

16. R. B. STEPHENS, D. A. STEINMAN, M. L. HOPPE, "White Light Interferometry for the Optical Characterization of Transparent ICF Shells," *Fusion Sci. Technol*. **49**, 646 (2006).

17. H. HUANG, R. B. STEPHENS, D. HILL, C. LYON, A. NIKROO, D. A. STEINMAN "Automated Batch Characterization of ICF Shells with Vision-Enabled Optical Microscope System," *Fusion Sci. Technol*. **45**, 214 (2004).

18. Filmetrics F20 Spectral Interferometer by Filmetrics, Inc., www.filmetrics.com

19. H. HUANG, R. B. STEPHENS, J. B. GIBSON, I. VALMIANSKI, "3D Surface Reconstruction of ICF Shells after Full Surface Spheremapping," *Fusion Sci. Technol*. **49**, 642 (2006).